

Oxalate-induced renal pyroptotic injury and crystal formation mediated by NLRP3-GSDMD signaling *in vitro* and *in vivo*

YUE CHEN^{1*}, SHUSHUAI YANG^{1*}, HAILONG KONG^{1*}, QI WANG^{1,2},
SHIQUN CHEN³, XINGYU WANG¹, LIQUN CHEN³ and SHIYONG QI¹

¹Department of Urology, The Second Hospital of Tianjin Medical University, Tianjin Institute of Urology, Tianjin 300211;

²Department of Thoracic Surgery, Jinshan Hospital of Fudan University, Shanghai 200540;

³Academy of Medical Engineering and Translational Medicine, Tianjin University, Tianjin 300072, P.R. China

Received June 27, 2023; Accepted August 31, 2023

DOI: 10.3892/mmr.2023.13096

Abstract. Calcium oxalate kidney stone has become an urgent issue due to its high incidence and recurrence rate. Thus, it is necessary to explore for mechanisms of calcium oxalate stones formation. Previous studies demonstrated that oxalate crystals could induce the activation of nucleotide-binding domain and leucine-rich repeat-containing family pyrin domain-containing 3 (NLRP3) inflammasome and change the renal tubular epithelium adhesion. However, the type and molecular mechanism of NLRP3 inflammasome-mediated calcium oxalate stones formation still need to be further investigated. In the present study, it was confirmed that the NLRP3-gasdermin D (GSDMD) signaling was involved in oxalate-induced cell injury *in vitro* and *in vivo*. Inhibition of reactive oxygen species production could effectively prevent the NLRP3 inflammasome formation in oxalate-treated HK-2 cells. NLRP3 gene silencing could inhibit the DNA damage and cellular membrane injury of HK-2 cells treated with oxalate. The ultrastructural changes of several organelles and particular structures, similar to typical cell pyroptosis, were observed in oxalate-stimulated HK-2 cells. NLRP3 gene silencing could antagonize the oxalate-induced injury and ultrastructure changes. Additionally, NSA (GSDMD inhibitor) could prevent the oxalate-induced injury of membrane integrity

in HK-2 cells. Moreover, oxalate crystals were significantly decreased in *GSDMD*^{-/-} mice compared with wild-type mice with glyoxylic acid. Together, NLRP3-GSDMD pathway was involved in the oxalate-induced pyroptotic injury in HK-2 cells. GSDMD and its cleavage form GSDMD-N played an important role in the oxalate-induced renal cell injury and oxalate calcium crystals formation *in vitro* and *in vivo*. This provided a new target for prevention and treatment of oxalate nephropathy and oxalate calcium stones.

Introduction

Nephrolithiasis is one of the common and important problems in daily urological practice. Among patients in different regions, calcium oxalate (CaOx) is an important component involved in the formation of kidney stone (1). CaOx stone has become an urgent issue due to its high incidence and recurrence rate (2). It had been demonstrated that oxalate metabolism was closely related to the occurrence and development of calcium oxalate stones disease (3). When oxalate homeostasis is disordered, a large amount of oxalate will accumulate in tissues, especially in kidney (4). It is already revealed that oxalate could result in the death of renal interstitial cells and basolateral cells (5). Additionally, a recent study demonstrated that cellular dysfunction and damage in HK-2 cells could be induced by oxalate exposure (6). Hence, it is fairly necessary to perform an in-depth exploration for molecular mechanisms of calcium oxalate kidney stones formation.

Several studies have demonstrated that the nucleotide-binding domain and leucine-rich repeat-containing family pyrin domain-containing 3 (NLRP3) inflammasome was involved in the onset and progression of calcium oxalate stones (7,8). NLRP3 inflammasome, a kind of cytoplasmic protein, is composed of NLRP3 receptor, apoptosis-associated speck-like protein (ASC) and procaspase-1 (9). Both intracellular and extracellular stimulations could activate the NLRP3 inflammasome by pathogen-associated molecular patterns and damage-associated molecular patterns (10). It has been demonstrated that procaspase-1 could be cleaved into its active form caspase-1 by the activation of NLRP3 inflammasome, which induces the maturity and secretion of IL-1 β and IL-18 (11,12). In addition, reactive oxygen species (ROS)

Correspondence to: Professor Shiyong Qi, Department of Urology, The Second Hospital of Tianjin Medical University, Tianjin Institute of Urology, 23 Pingjiang Road, Hexi, Tianjin 300211, P.R. China
E-mail: qsymanu@126.com

Professor Liqun Chen, Academy of Medical Engineering and Translational Medicine, Tianjin University, 92 Weijin Road, Nankai, Tianjin 300072, P.R. China
E-mail: liqun.chen@tju.edu.cn

*Contributed equally

Key words: calcium oxalate stone, pyroptosis, gasdermin D, nucleotide-binding domain and leucine-rich repeat-containing family pyrin domain-containing 3, reactive oxygen species

production have been proved to be involved in the activation of NLRP3 inflammasome (13). A previous study conducted by the authors demonstrated that calcium oxalate monohydrate could induce the activation of NLRP3 inflammasome and change the adhesion of renal tubular epithelium to calcium oxalate crystals (14). However, the type and mechanism of NLRP3 inflammasome-mediated calcium oxalate stones formation still need deeper investigation.

Currently, cell pyroptosis was proved as programmed cell death characterized by nuclear pyknosis and DNA fragmentation (15). Previous studies have illustrated that oxalate crystals-induced injury was a kind of programmed cell death (16,17). The classical pathway of pyroptosis was described as a pathway centered on caspase-1 activation, which was mediated by inflammasome (18). Gasdermin D (GSDMD), a member of gasdermin protein family, is the substrate protein of all inflammatory caspases (18). It was previously reported that the activated GSDMD was cleaved into GSDMD-N by inflammatory caspase (such as caspase-1), which was involved in the formation of membrane pores (18,19). Through the membrane pores mediated by GSDMD-N, extracellular materials could enter the cells and the intracellular components also be released into intercellular environment, which will subsequently cause the swelling and deformation of cells (20). Although a number of studies explained the association between oxalate calcium crystals and NLRP3-GSDMD pathway and its potential therapeutic targets (21,22), ultrastructural characteristics and intensive mechanisms of GSDMD-induced cell pyroptosis in oxalate calcium crystals formation are still not completely clear.

Materials and methods

Cell culture. HK-2 cells were purchased from Shanghai Institutes for Biological Sciences (Shanghai, China) and cultured in high glucose DMEM supplemented with 10% fetal bovine serum and 1% penicillin/streptomycin (all purchased from Gibco; Thermo Fisher Scientific, Inc.). Cells were incubated in 37°C and 5% CO₂. A total of 20 mM primary solution of oxalate (MilliporeSigma; Merck KGaA) was prepared in phosphate buffered saline (PBS), and applied within 1 week with a pH number of 7.2-7.4. HK-2 cells were treated with oxalate at different concentrations (0.1, 0.2, 0.4, 0.6, 0.8, 1.0 and 2.0 mM) for 24 h, and then cells were separately collected or treated for further experiments. Necrosulfonamide (NSA) (MedChemExpress), an inhibitor of GSDMD-N, was diluted in dimethyl sulphoxide (DMSO) (Tianjin Solomon Biotechnology Co., Ltd.) and pretreated HK-2 cells at the concentrations of 5 and 15 μM for 2 h.

Cell Counting Kit-8 (CCK-8) assay. HK-2 cell viability was examined through CCK-8 assay. HK-2 cells (4x10³) were seeded in 96-well plates and then treated with oxalate at different concentrations (0.1, 0.2, 0.4, 0.6, 0.8, 1.0 and 2.0 mM) for 24 h. After the cells were incubated with CCK-8 solution (10 μl; GlpBio Technology) for 2 h, the optical density was measured by a microplate reader at 450 nm absorption wavelength.

Lactate dehydrogenase (LDH) release. The concentration of LDH in culture medium after oxalate treatment was detected by LDH release assay. N-acetyl cysteine (NAC) (MilliporeSigma;

Merck KGaA), a scavenger of ROS, was prepared in PBS and pretreated HK-2 cells for 2 h. HK-2 cells (1x10⁵) were incubated with oxalate in 6-well plates at 37°C for 24 h at different concentrations (0.1, 0.2, 0.4, 0.6, 0.8, 1.0 and 2.0 mM) after the pretreatment with NAC or NSA for 2 h at 37°C. The concentration of LDH in medium was examined by LDH-kit (Nanjing Jiancheng Bioengineering Institute) according to the manufacturer's instructions. The optical density was detected by a microplate reader at 450 nm absorption wavelength.

Detection of ROS production. HK-2 cells (1.5x10⁴) were seeded in 24-well plates and incubated with oxalate (0.8 mM) for 24 h at 37°C after pretreatment with NSA. ROS production in HK-2 cells was detected using 10 μM dichlorofluorescein diacetate (DCF-DA) (Beyotime Institute of Biotechnology) following the manufacturer's protocol. Finally, the detection of DCF fluorescence was carried out at 488 nm excitation and 525 nm emission wavelengths using a fluorescence microscope.

TUNEL staining. Oxalate-induced nuclear DNA damage was detected by TUNEL Apoptosis Assay Kit (Beyotime Institute of Biotechnology) according to the manufacturer's instructions. HK-2 cells (1.5x10⁴) were seeded in 24-well plates and incubated with oxalate (0.8 mM) for 24 h at 37°C after pretreatment with NSA for 2 h or after NLRP3 gene silencing. Cells were washed with PBS three times and fixed with 4% paraformaldehyde for 30 min at room temperature, followed by permeabilization with 0.1% Triton X-100 for 5 min. After washing, cells were stained with 50 μl TUNEL working solution for 60 min at 37°C, and nuclei were stained with 5 μg/ml DAPI for 5 min at room temperature. After washing, one drop of Antifade Mounting Medium (Beijing Solarbio Science & Technology Co., Ltd.) was added and then the coverslip was added. Oxalate-induced nuclear DNA damage was detected by TUNEL Apoptosis Assay Kit (cat. no. C1088; Beyotime Institute of Biotechnology) according to the manufacturer's instructions. The cellular fluorescence intensities were observed through a confocal microscope and 4 fields of view for every group were recorded.

Calcein-AM/PI staining. Oxalate-induced cell death in HK-2 cells was detected by Calcein-AM/PI Double Stain Kit (Tianjin Solomon Biotechnology Co., Ltd.) according to the manufacturer's protocol. HK-2 cells (1.5x10⁴) were seeded in 24-well plates and incubated with oxalate (0.8 mM) for 24 h at 37°C after pretreatment with NSA for 2 h or after NLRP3 gene silencing. Thereafter, cells were stained with 2 μM Calcein-AM and 5 μM PI for 15 min at 37°C, and nuclei were stained with 5 μg/ml DAPI for 5 min at room temperature. Oxalate-induced cell death in HK-2 cells was detected by Calcein-AM/PI Double Stain Kit (cat. no. CA1630; Tianjin Solomon Biotechnology Co., Ltd.) according to the manufacturer's protocol. The cellular fluorescence intensities were observed through a confocal microscope.

Small interfering RNA (siRNA) knockdown experiments. Double-stranded siRNA targeting NLRP3 gene and negative control (NC) siRNA were purchased from Shanghai GenePharma Co., Ltd. HK-2 cells were transfected using

siRNA mixed with Lipofectamine 2000 (Invitrogen; Thermo Fisher Scientific, Inc.) according to the manufacturer's protocol. Subsequently, HK-2 cells (1×10^5) were incubated with oxalate (0.8 mM) in 6-well plates for 24 h at 37°C. Then, HK-2 cells were transfected using 100 pM siRNA mixed with 5 μ l Lipofectamine 2000 (Invitrogen; Thermo Fisher Scientific, Inc.) for 6 h at 37°C according to the manufacturer's protocol. Subsequent experiments were performed 48 h after transfection. The sequences used were as follows: NLRP3-siRNA forward, 5'-GGAGAGACCUUUAUGAGAATT-3' and reverse, 5'-UUCUCAUAAAGGUCUCUCCTT-3'; and negative control (NC) forward, 5'-UUCUCCGAACGUGUCACGUTT-3' and reverse, 5'-ACGUGACACGUUCGGAGAATT-3'.

Reverse transcription-quantitative PCR (RT-qPCR). The total RNA from HK-2 cells was extracted by TRIzol reagent (Invitrogen; Thermo Fisher Scientific, Inc.) and cDNA was then synthesized using reverse transcription system kit (cat. no. K1691; Thermo Fisher Scientific, Inc.) according to the manufacturer's instructions. RT-qPCR was performed using the SYBR Premix Ex Taq II (Takara Biotechnology Co., Ltd.) following the manufacturer's protocols. The specific RT-qPCR primer sequences were as follows: NLRP3 forward, 5'-CGT GAGTCCCATTAAGATGGAGT-3' and reverse, 5'-CCCGAC AGTGGATATAGAACAGA-3'; caspase-1 forward, 5'-TTT CCGCAAGGTTTCGATTTTCA-3' and reverse, 5'-GGCATC TGCGTCTACCATC-3'; IL-1 β forward, 5'-AGCTACGAA TCTCCGACCAC-3' and reverse, 5'-CGTTATCCCATGTGT CGAAGAA-3'; and GAPDH forward, 5'-GAAGGTGAAGGT CGGAGT-3' and reverse, 5'-GAAGATGGTGATGGGATT TC-3'. The thermocycling conditions for RT-qPCR were as follows: 95°C initial denaturation for 3 min, followed by 45 cycles of denaturation at 95°C for 30 sec, annealing at 50–60°C for 30 sec and extension at 72°C for 30 sec. The amplification and analysis were performed on a real-time PCR system (Applied Biosystems™ 7500 Real-Time PCR System; Applied Biosystems; Thermo Fisher Scientific, Inc.). All of the data were analyzed with the $2^{-\Delta\Delta C_q}$ method (23) and normalized using GAPDH cDNA as internal control.

Western blot analysis. Proteins from HK-2 cells or mice kidney tissue were lysed in RIPA lysis buffer (Beijing Solarbio Science & Technology Co., Ltd.) containing the protease inhibitor cocktail (Roche Diagnostics), and protein concentrations were determined referring to bovine serum albumin standard using the bicinchoninic acid method. The same amounts of proteins (50 μ g) were separated on 10–12% gels using sodium dodecyl sulfate-polyacrylamide gel electrophoresis and transferred to nitrocellulose membranes, followed by western blotting as previously described (14). Membranes were washed using TBST containing 0.1% Tween 20. After blocking with 5% skimmed milk for 1 h at room temperature, the membranes were incubated with primary antibodies in 4°C overnight. After extensive washing, blots were incubated with secondary antibodies for 1 h at room temperature. The bands were developed using Pierce™ ECL Western blotting substrate (Thermo Fisher Scientific, Inc.). Primary antibodies were against GSDMD (cat. no. 20770-1-AP; 1:500; Proteintech Group, Inc.), GSDMD-N (cat. nos. DF12275 and DF13758; 1:1,000; Affinity Biosciences), NLRP3 (cat. no. ab263899;

1:1,000; Abcam), Caspase-1 (cat. no. ab179515; 1:1,000; Abcam), IL-1 β (cat. no. ab283818; 1:1,000; Abcam), IL-18 (cat. no. 10663-1-AP; 1:2,000; Proteintech Group, Inc.), osteopontin (OPN) (cat. no. sc-21742; 1:200; Santa Cruz Biotechnology, Inc.) and GAPDH (cat. no. sc-365062; 1:200; Santa Cruz Biotechnology, Inc.) as a reference protein. Anti-rabbit (cat. no. SC-2357; 1:2,000) and anti-mouse (cat. no. SC-516102; 1:2,000) IgG secondary antibodies were purchased from Santa Cruz Biotechnology, Inc.

Transmission electron microscopy (TEM). After incubation with oxalate (0.8 mM) for 24 h, HK-2 cells transfected with NLRP3-siRNA or scrambled-siRNA were collected and fixed in 2.5% glutaraldehyde for 2 h at room temperature. After washing three times with PBS, postfixation staining was performed using 1% osmium tetroxide for 1 h at room temperature. Furthermore, cells were dehydrated in gradient ethanol solution and treated with propylene oxide, Spurr's low viscosity resin for 18 h. Cells were further treated with pure resin for 24 h and embedded in Beem capsules. Resin blocks were hardened at 70°C for 2 days. Ultra-thin slices (70 nm) were prepared and stained with 1% lead citrate and 0.5% uranyl acetate after the processes of dehydration, embedding, infiltration and slicing following the manufacturer's protocol. Ultrathin sections were observed using HT7700 Transmission Electron Microscopy (Hitachi, Ltd.).

Animal experiments. C57BL/6 (6-week old; mean weight, 20 g) male mice were purchased from the Vital River Laboratories (Beijing, China). *GSDMD*^{-/-} mice were obtained from the Chen's Lab in Tianjin University. *GSDMD*^{-/-} mice were obtained from heterozygous *GSDMD*^{+/-} mice intercross confirmed by genotyping. All mice were maintained and treated in accordance with the Animal Ethics Committee at the Second Hospital of Tianjin Medical University (Tianjin, China; approval no. KY2022K103). All mice were housed under 25°C and 30% humidity conditions with an equal light/dark cycle, and raised with free access to specialized feed and water. The oxalate nephropathy model was induced through intraperitoneal injection of 0.8% glyoxylic acid (Gly) (Shanghai Macklin Biochemical Co., Ltd.). Two groups of 10 mice each were randomly divided into the control group and the Gly group. The mice were sacrificed through cervical dislocation after Gly treatment for 7 days. The kidney, plasma and urine specimens were collected after treatment for 7 days. The kidneys were washed twice with 0.9% normal saline and were dried on the absorbent paper. Subsequently, the kidneys were weighed with a 1/10,000 analytical balance. All samples were stored at -80°C or fixed for subsequent experiments.

Histological staining and biochemical examination. The cross section of the kidney specimen was obtained after the kidney tissues were fixed, embedded and positioned. Mouse kidney tissues were fixed in 4% paraformaldehyde overnight at room temperature and paraffin embedded. Sections (5 μ m) were stained with hematoxylin for 5 min and eosin for 3 min at room temperature, and then observed by light microscope (Nikon Corporation). The sections were stained with haematoxylin and eosin (H&E) for basic histological examination. The oxalate crystals were observed through

Von Kossa staining (cat. no. G3282; Beijing Solarbio Science & Technology Co., Ltd.). For tissue immunostaining, mouse kidneys were dissected, fixed with buffered 4% paraformaldehyde overnight at 4°C, cryoprotected in 30% sucrose solution overnight, and finally embedded in optimal cutting temperature compound. The immunohistochemistry (IHC) staining was performed with specific primary antibodies against the target proteins for 1 h at room temperature. Primary antibodies were against NLRP3 (cat. no. 68102-1-Ig; 1:50; Proteintech Group, Inc.), Caspase-1 (cat. no. ab138483; 1:100; Abcam), GSDMD (cat. no. 20770-1-AP; 1:50; Proteintech Group, Inc.), GSDMD-N (cat. no. DF13758; 1:50; Affinity Biosciences), IL-1 β (cat. no. ab283818; 1:100; Abcam), IL-18 (cat. no. 10663-1-AP; 1:50; Proteintech Group, Inc.) and osteopontin (OPN) (cat. no. sc-21742; 1:50, Santa Cruz Biotechnology, Inc.). Anti-rabbit (cat. no. SC-2357; 1:5,000; Santa Cruz Biotechnology, Inc.) and anti-mouse (cat. no. SC-516102; 1:5,000; Santa Cruz Biotechnology, Inc.) IgG secondary antibodies were applied. Serum creatinine was detected using Creatinine Quantitative Colorimetric kit (cat. no. BC4910; Beijing Solarbio Science & Technology Co., Ltd.) according to the manufacturer's instructions.

Quantification of image. The intensity of fluorescence or autoradiogram in cellular/histological staining and western blotting assays was quantified with the software ImageJ (version 1.8.0; National Institutes of Health). Quantified data were normalized with those of the control, and then were plotted as bar charts.

Statistical analysis. Statistical analysis was performed through statistical software (SPSS v20.0; IBM Corp.) and the experimental data were analyzed using an independent unpaired t-test or one-way ANOVA. LSD test was used as a post hoc test for comparison between groups following one-way ANOVA. Each experiment was conducted for 4–6 repeats and the data are presented as the mean \pm standard error. All results with two-side $P < 0.05$ were considered to indicate a statistically significant difference.

Results

Oxalate induces the formation of NLRP3 inflammasome in HK-2 cells. In order to confirm the role of NLRP3 inflammasome in the occurrence and development of calcium oxalate renal stones, the viability in HK-2 cells treated with oxalate at different concentrations (0.1, 0.2, 0.4, 0.6, 0.8, 1.0 and 2.0 mM) was firstly evaluated. The bar graph revealed that oxalate did not reduce the viability of HK-2 cells at concentrations less than 1.0 mM (at 0.1, 0.2, 0.4, 0.6 and 0.8 mM) after treatment for 24 h (Fig. 1A). Meanwhile, the LDH levels in cell medium in HK-2 cells treated with oxalate at different concentrations (0.1, 0.2, 0.4, 0.6, 0.8, 1.0 and 2.0 mM) were measured. As illustrated in Fig. 1B, oxalate treatment increased LDH release in a dose-dependent manner, compared with the control cells, especially at higher oxalate concentration (0.8, 1.0 and 2.0 mM), suggesting cell membrane injury in oxalate-treated HK-2 cells. Thus, 0.8 mM was selected as treatment concentration of oxalate in the present study. Furthermore, the transcription and translation levels of NLRP3, caspase-1 and

IL-1 β were detected in HK-2 cells with 0.8 mM oxalate treatment. The results of RT-qPCR and western blot assays revealed that the mRNA and protein levels of NLRP3, caspase-1 and IL-1 β significantly increased in oxalate-treated HK-2 cells, compared with the control cells (Figs. 1C and D and S1). These results suggested that NLRP3 inflammasome was formed in oxalate-treated HK-2 cells.

Oxalate-induced activation of NLRP3 inflammasome is mediated by ROS production. ROS is known to be involved in the activation of NLRP3 inflammasome (24). To identify the possible contribution of ROS production in oxalate-induced activation of NLRP3 inflammasome, the ROS production in HK-2 cells after oxalate treatment was detected. NAC, a scavenger of the production of ROS, was non-cytotoxic to HK-2 cells at 1, 3, 5 and 8 mM, compared with the untreated control cells (Fig. 2A). The fluorescence images demonstrated that 0.8 mM oxalate could significantly induce ROS production, while 5 mM NAC decreased ROS level in oxalate-treated HK-2 cells (Figs. 2B and S2). In addition, the protein contents of NLRP3 were detected to define the role of ROS in activation of NLRP3 inflammasome through NAC treatment. As revealed in Fig. 2C, NAC (5 mM) could inhibit the expression level of NLRP3 induced by oxalate treatment in HK-2 cells (Figs. 2C and S3). Collectively, the aforementioned results demonstrated that oxalate-induced formation of NLRP3 inflammasome was mediated by ROS production.

Oxalate can induce injury of HK-2 cells mediated by NLRP3. A previous study suggested that oxalate could induce rat renal tubular epithelial cells injury, which was a type of programmed cell death (16). Different from apoptosis, classical pyroptosis pathway depends on the sheared GSDMD activated by NLRP3-caspase-1 signaling, which participated in oxalate induced renal injury and renal crystals (21). In the present study, western blot analysis results revealed that the protein levels of NLRP3 and caspase-1 were significantly increased in oxalate-treated HK-2 cells (Figs. 3A and S4). Meanwhile, the NLRP3 and caspase-1 concentrations could be prevented after NLRP3 gene silencing in HK-2 cells (Figs. 3A and S4). Additionally, LDH release was decreased in NLRP3-knocked down HK-2 cells treated with oxalate compared with scrambled control, which suggested disrupted integrity of cell membrane (Fig. 3B). Pyroptosis is characterized by nuclear pyknosis, cell swelling and membrane rupture (25). By TUNEL staining and Calcein-AM/PI staining, it was observed that oxalate could induce the fragmentation of nuclear DNA and the death of HK-2 cells (Figs. 3C and D, S5 and S6). At the same time, it was revealed that the oxalate-induced morphological changes in HK-2 cells could be protected by NLRP3 gene silencing (Figs. 3C and D, S5 and S6). Based on the aforementioned results, it has been suggested that the oxalate-induced injury in HK-2 cells was a kind of programmed cell death, which was mediated by NLRP3 signaling and characterized with the fragmentation of nuclear DNA and the disruption of cell membrane integrity, and all the features were consistent with pyroptosis.

Ultrastructural changes of oxalate-induced pyroptotic injury in HK-2 cells. Previous studies have demonstrated the fragmentation of nuclear DNA and the disruption of

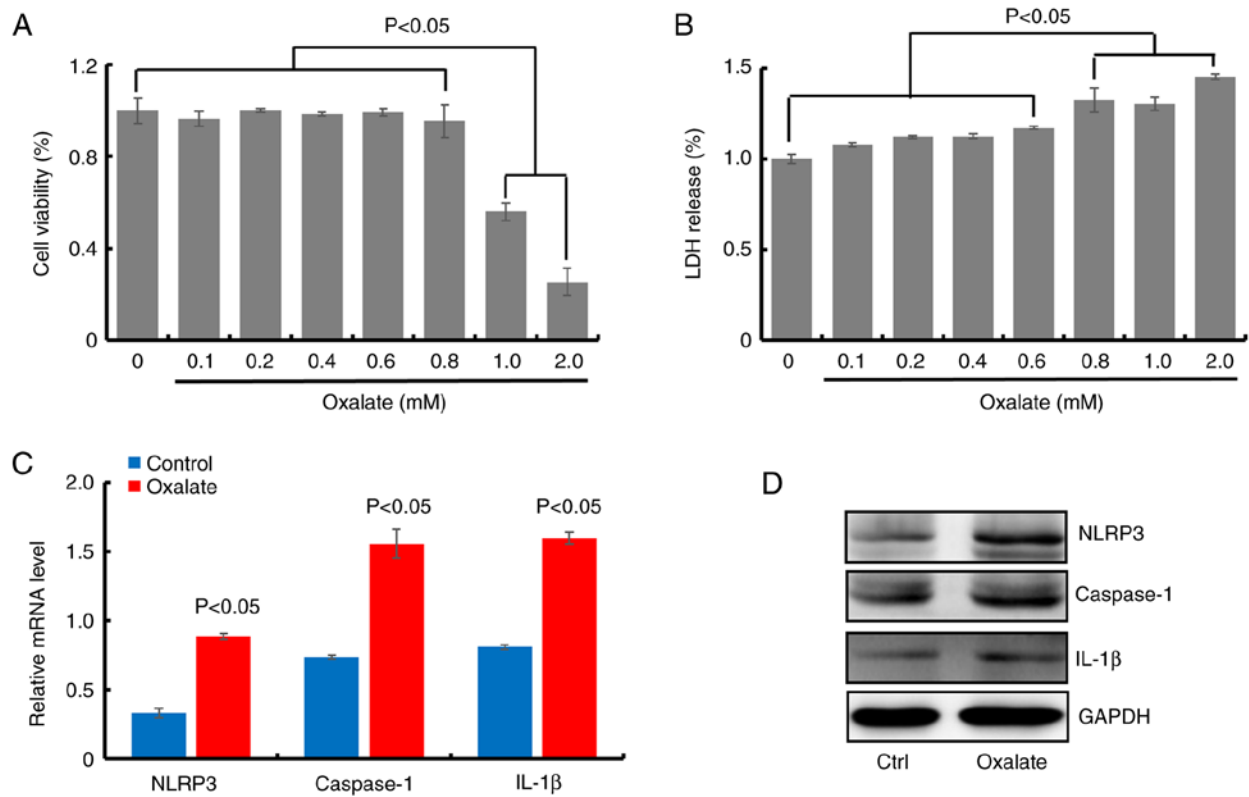


Figure 1. NLRP3 inflammasome forms in HK-2 cells treated with oxalate. (A) Cell viability was detected through the Cell Counting Kit-8 assay in HK-2 cells treated with oxalate at different concentrations for 24 h (n=6). (B) Lactate dehydrogenase levels were evaluated in HK-2 cells treated with various concentrations of oxalate (n=6). (C) mRNA expression levels of NLRP3, caspase-1 and IL-1 β in HK-2 cells treated with 0.8 mM oxalate for 24 h, as measured by reverse transcription-quantitative PCR assay (n=4). (D) Western blot analysis of NLRP3, caspase-1 and IL-1 β protein levels in HK-2 cells upon exposure to 0.8 mM oxalate for 24 h. NLRP3, leucine-rich repeat-containing family pyrin domain-containing 3; Ctrl, control.

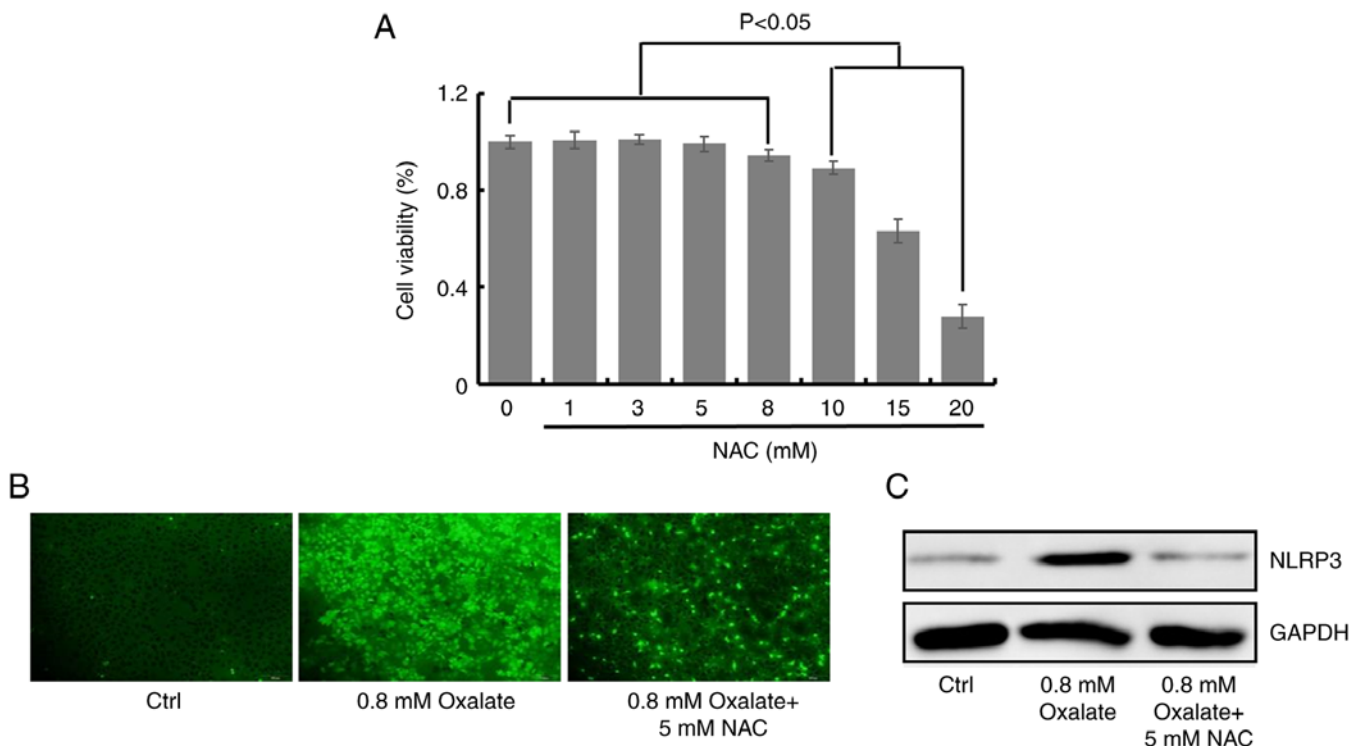


Figure 2. Oxalate induces NLRP3 activation through reactive oxygen species. (A) Cell viability was evaluated with the Cell Counting Kit-8 assay in HK-2 cells dealt with NAC at various concentrations for 24 h (n=6). (B) Images of green color in HK-2 cells with 10 μ M DCF-DA staining observed by fluorescence microscope. After pretreatment with 5 mM NSA, cells were treated with oxalate at 0.8 mM for 24 h followed by staining. Magnification, x20. (C) The protein levels of NLRP3 in HK-2 cells treated with 5 mM NSA 0.8 mM oxalate for 24 h was detected by western blotting. NLRP3, leucine-rich repeat-containing family pyrin domain-containing 3; NAC, N-acetyl cysteine; DCF-DA, dichlorofluorescein diacetate; NSA, necrosulfonamide; Ctrl, control.

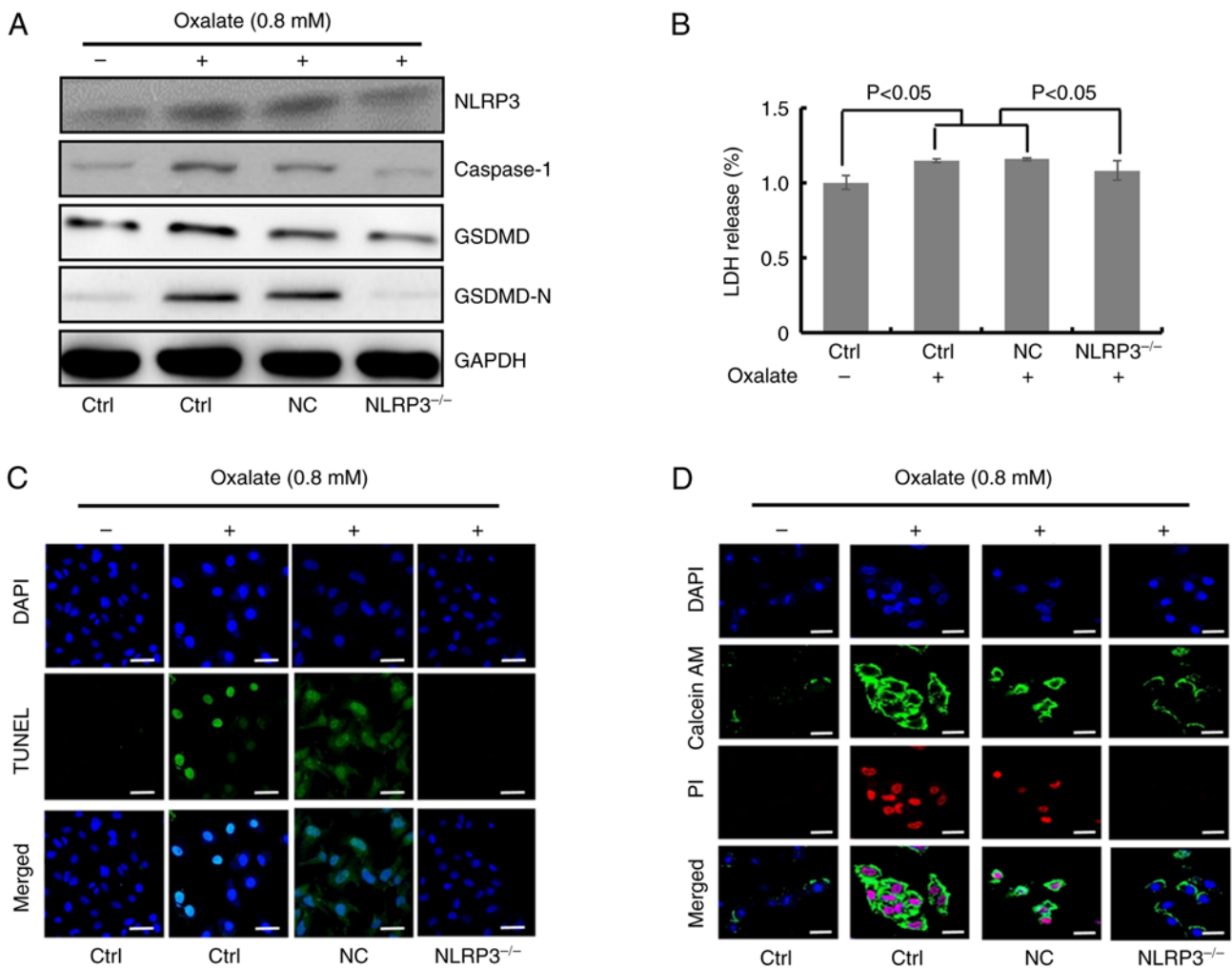


Figure 3. NLRP3 knockdown ameliorates oxalate-caused injury of HK-2 cells. (A) Western blot detection of NLRP3, caspase-1, GSDMD and GSDMD-N protein contents in HK-2 cells treated with 0.8 mM oxalate for 24 h after transfection with NLRP3-siRNA. (B) Relative lactate dehydrogenase levels in HK-2 cells transfected with NLRP3-siRNA upon 0.8 mM oxalate treatment for 24 h (n=6). (C) Images of two colors (blue and green) and merged colors in HK-2 cells with TUNEL staining were observed by confocal microscopy. HK-2 cells with NLRP3 silence were treated with 0.8 mM oxalate for 24 h followed by staining. Scale bars, 100 μ m. (D) Images of three colors (blue, green and red) and merged colors in HK-2 cells with Calcein-AM/PI staining were recorded through confocal microscopy. HK-2 cells transfected with NLRP3-siRNA or scrambled-siRNA were dealt with 0.8 mM oxalate for 24 h. Scale bars, 100 μ m. NLRP3, leucine-rich repeat-containing family pyrin domain-containing 3; GSDMD, gasdermin D; siRNA, small interfering RNA; Ctrl, control; NC, negative control.

cell membrane integrity in oxalate-induced HK-2 cells. Numerous morphological changes are typical features of pyroptosis (26). In order to explore the ultrastructural changes of oxalate-induced injury in HK-2 cells, the HK-2 cells with different treatment through TEM were observed. The TEM images revealed that the structures of several organelles in the oxalate-treated HK-2 cells were changed. As demonstrated in electron micrograph, mitochondrial cristae was disrupted and disappeared (Fig. 4A), Golgi apparatus became swollen and hypertrophic (Fig. 4B), rough endoplasmic reticulum was slender and shallow (Fig. 4C) and microvilli appeared thick and short (Fig. 4D). Furthermore, all these injuries of organelles could be ameliorated in HK-2 cells subjected to NLRP3 gene silencing (Fig. 4A-D). In addition, certain particular ultra-structures in HK-2 cells after oxalate treatment were also observed. As displayed in Fig. 5, autophagosomes, oxalate crystal phagosomes, vacuoles and membrane pores appeared in cytoplasm and cell membrane of HK-2 cells. Moreover, these abnormal structures in oxalate treated HK-2 cells could

be repaired by NLRP3 gene silencing (Fig. 5A-D). These findings suggested that oxalate induced a series of ultrastructural injuries in HK-2 cells organelles, similar to typical changes of pyroptosis.

GSDMD is involved in the oxalate-induced renal cell injury and oxalate crystals formation in vitro and in vivo. The aforementioned experiments had confirmed that the features of oxalate-induced injury in HK-2 cells, which was consistent with pyroptosis. It has been reported that GSDMD can be cleaved into GSDMD-N to induce cell pyroptosis (18). In order to clarify the role of GSDMD in oxalate-induced HK-2 cell injury, the influences of NSA on oxalate-stimulated HK-2 cells *in vitro* were detected. NSA, is an inhibitor of the protein function of GSDMD-N which inhibits GSDMD-N oligomerization. As illustrated in Fig. 6A, there was not toxicity in HK-2 cells incubated with 5 and 15 μ M NSA or DMSO solvent. However, NSA could prevent the oxalate-induced LDH-release in HK-2 cells at 15 μ M (Fig. 6A). Meanwhile, western blot results

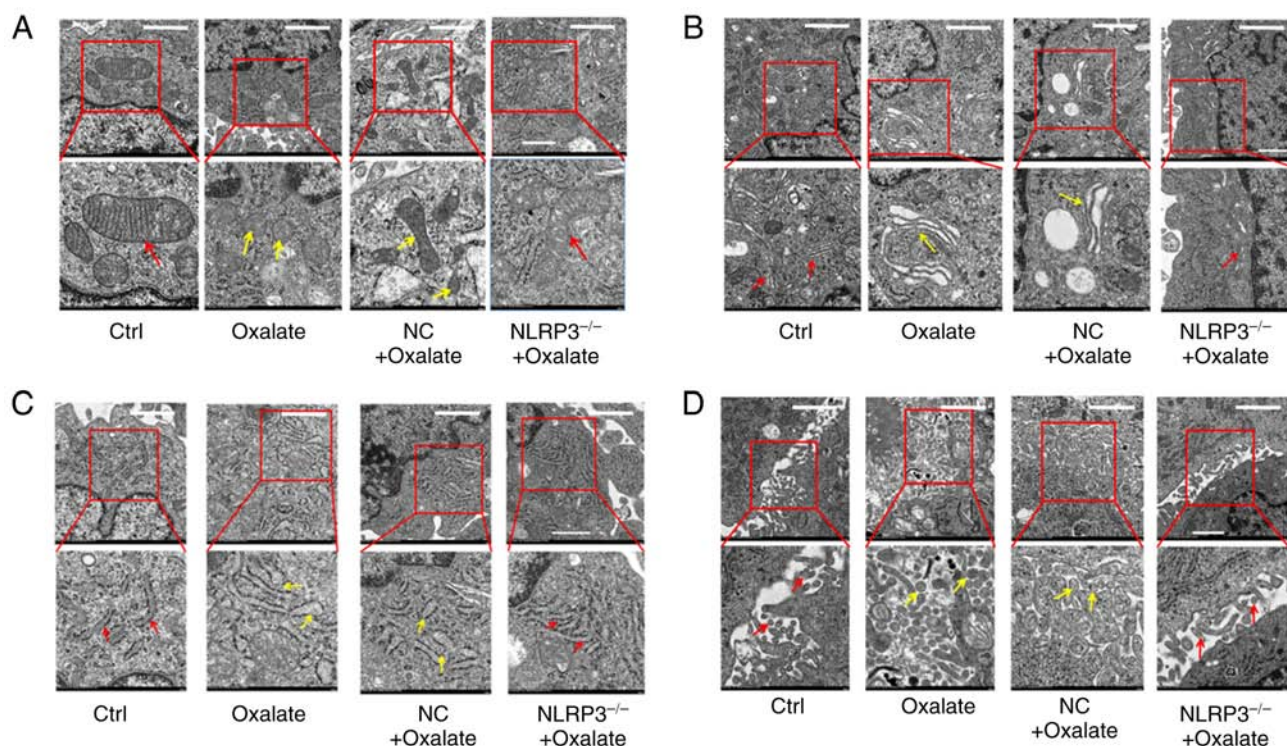


Figure 4. Injury of organelles in oxalate-stimulated HK-2 cells. (A-D) Representative transmission electron microscopy image of (A) mitochondrial, (B) Golgi apparatus, (C) endoplasmic reticulum and (D) microvilli in HK-2 cells. HK-2 cells transfected with NLRP3-siRNA or scrambled-siRNA were treated with 0.8 mM oxalate for 24 h. Scale bar, 1 μ m. NLRP3, leucine-rich repeat-containing family pyrin domain-containing 3; siRNA, small interfering RNA; Ctrl, control; NC, negative control.

revealed that oxalate could significantly increase the expression levels of NLRP3, caspase-1, GSDMD and GSDMD-N, and 15 μ M NSA treatment could inhibit the protein concentration of GSDMD, GSDMD-N and caspase-1 (Figs. 6B and S7). Additionally, TUNEL staining results demonstrated that NSA could not alleviate the fragmentation of nuclear DNA in HK-2 cells after oxalate treatment (Figs. 6C and S8), but NSA could decrease the oxalate-stimulated PI positive HK-2 cells through Calcein-AM/PI staining (Figs. 6D and S9). Based on the aforementioned results, it was concluded that GSDMD and GSDMD-N were involved in oxalate-induced pyroptosis of HK-2 cells, which could be prevented by NSA.

To confirm the role of GSDMD in oxalate calcium crystals formation *in vivo*, oxalate crystals animal model in C57BL/6 mice was first constructed using Gly. The Von Kossa staining showed obvious oxalate crystals in kidney of mice treated with Gly, compared with the untreated mice (Fig. 7A). Histological examination revealed considerable injury in Gly-treated mice through H&E staining, including epithelial cell swelling, renal tubule edema and neutrophil infiltration (Fig. 7B). In addition, the results of biochemical examination revealed higher blood creatinine in oxalate crystal mice (Fig. 7C). Moreover, western blot analysis for harvested kidneys revealed that a series of proteins of the NLRP3-GSDMD pathway (NLRP3, caspase-1, GSDMD, IL-1 β , IL-18 and OPN) were significantly increased in Gly-treated mice (Figs. 7D and S10). Furthermore, the similar alterations of these proteins were verified through IHC staining of the collected kidneys (Figs. 7E and S11). Collectively, these *in vivo* findings indicated that NLRP3-GSDMD signaling was involved in oxalate-stimulated renal pyroptotic injury.

Furthermore, oxalate crystals models in C57BL/6 wild-type (WT) mice and *GSDMD*^{-/-} mice were established. As revealed in Fig. 8A, oxalate crystals were significantly decreased in *GSDMD*^{-/-} mice with glyoxylic acid, compared with WT mice. Simultaneously, the level of blood creatinine was decreased in *GSDMD*^{-/-} mice compared with the WT mice treated with Gly (Fig. 8B). After the mice were sacrificed, IHC staining and western blotting were performed to detect the kidney protein levels in NLRP3-GSDMD pathway (Figs. 8C and D, S12 and S13). These results exhibited that GSDMD deficiency decreased the protein concentrations of NLRP3, caspase-1, IL-1 β , IL-18 and OPN in *GSDMD*^{-/-} mice in comparison with those in WT+Gly mice, suggesting GSDMD prevented Gly-induced oxalate crystal formation and the activation of NLRP3-GSDMD signaling *in vivo*. Collectively, the aforementioned findings illustrated the crucial impact of GSDMD on oxalate crystal formation.

Discussion

Based on previous studies, 5-15% of the population suffers from kidney stones throughout their lifetime, and >80% of kidney stones are calcium oxalate stones (27,28). Numerous studies have been performed to explore the pathogenesis of calcium oxalate stones in recent years. At present, a few factors are considered to contribute to calcium oxalate kidney stones, including lifestyle, hereditary and metabolism (1,3). Meanwhile, accumulating studies suggested oxidative stress and inflammatory injury was associated with calcium oxalate stones (29,30). Furthermore, a number of different studies

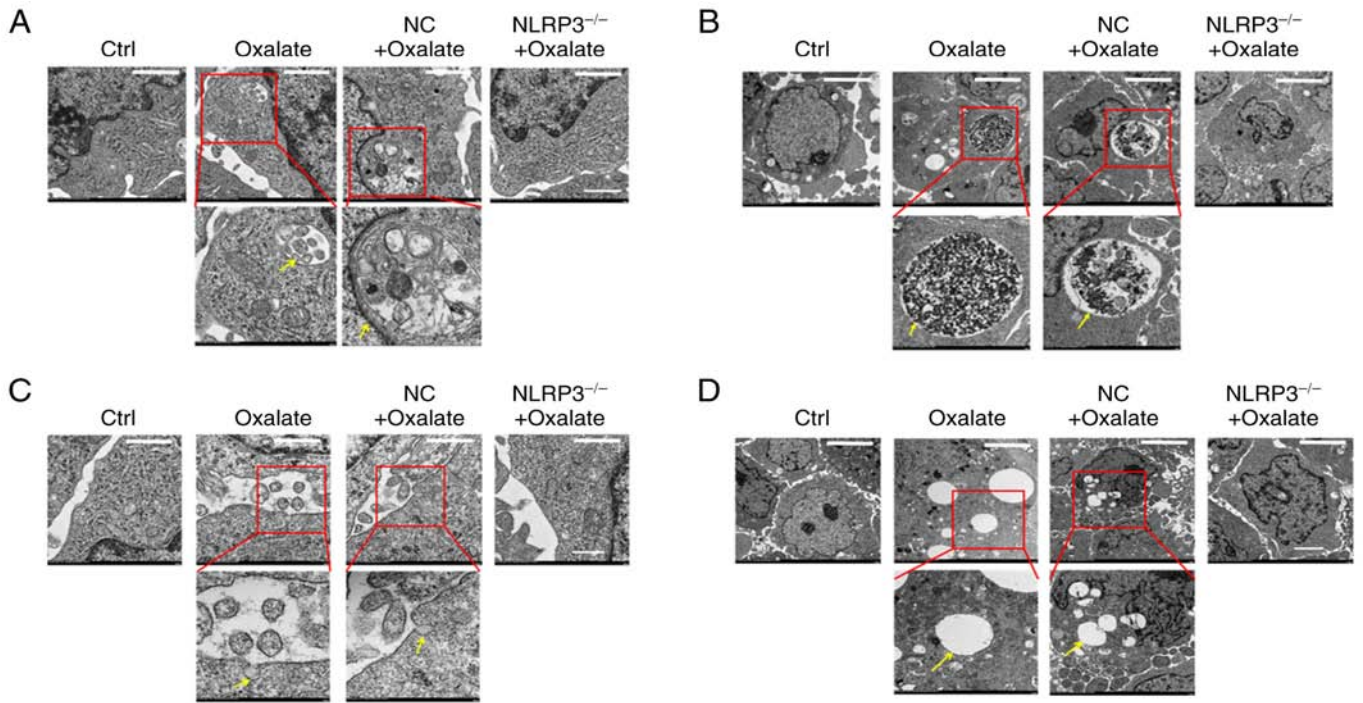


Figure 5. Ultrastructural changes in HK-2 cells treated with oxalate. (A) Autophagosomes, (B) oxalate crystal phagosomes, (C) membrane pores and (D) vacuoles emerged in cytoplasm and cell membrane of HK-2 cells through transmission electron microscopy observation. After transfection with NLRP3-siRNA or scrambled-siRNA, HK-2 cells were stimulated with 0.8 mM oxalate for 24 h. Scale bar, 1 μ m. NLRP3, leucine-rich repeat-containing family pyrin domain-containing 3; siRNA, small interfering RNA; Ctrl, control; NC, negative control.

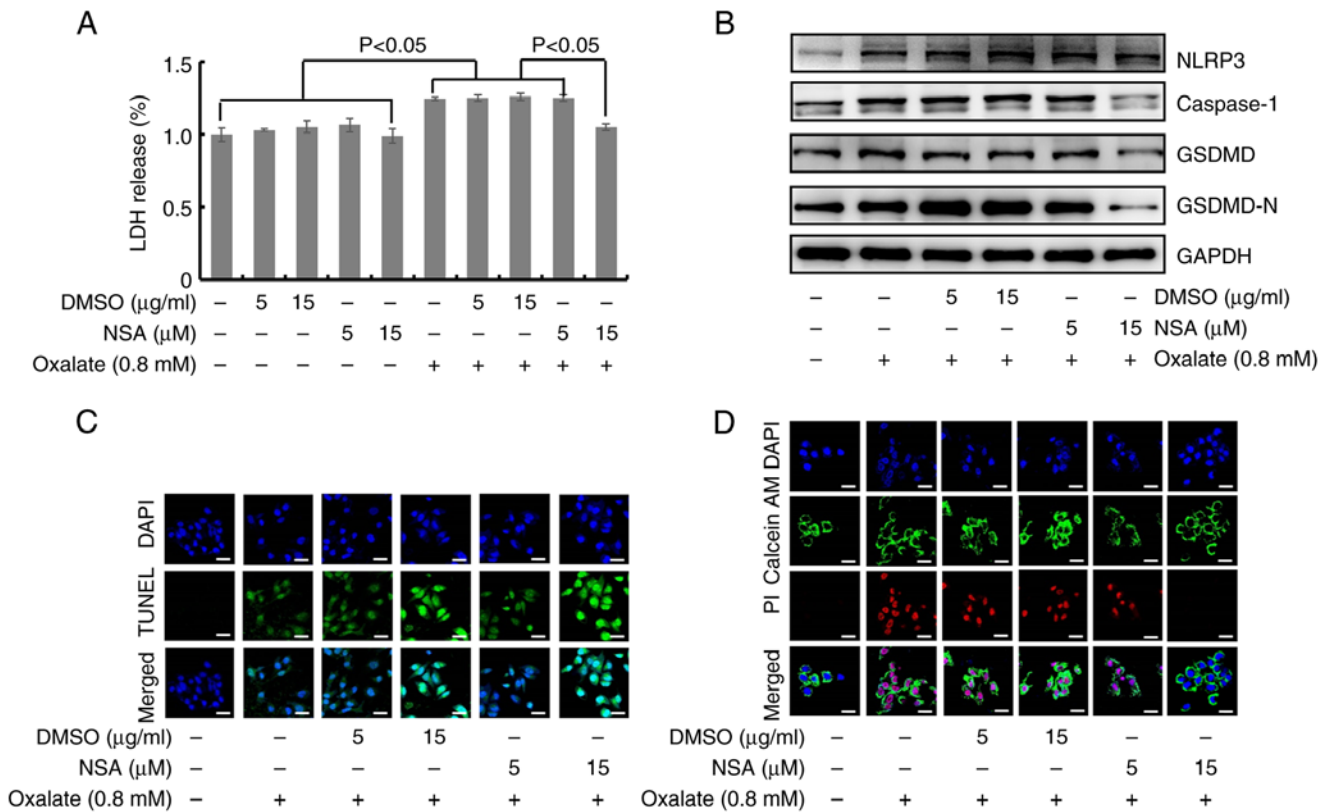


Figure 6. GSDMD is involved in oxalate-induced HK-2 cells pyroptotic injury. (A) Lactate dehydrogenase levels were examined in HK-2 cells treated with 0.8 mM oxalate and/or different concentrations of NSA for 24 h (n=6). (B) Protein contents detection of NLRP3, caspase-1, GSDMD and GSDMD-N in HK-2 cells treated with 0.8 mM oxalate and/or NSA (5 μ M and 15 μ M) for 24 h. (C) HK-2 was treated with 0.8 mM oxalate and/or NSA (5 and 15 μ M) for 24 h. Damaged nuclear DNA staining with TUNEL (shown in green) was observed by confocal microscopy. Cell nuclei were stained with DAPI (shown in blue). Scale bars, 100 μ m. (D) Living cells and dead cells staining with Calcein-AM (shown in green) and PI (shown in red) were examined through confocal microscopy. Cell nuclei were stained with DAPI (shown in blue). HK-2 was dealt with 0.8 mM oxalate and/or NSA (5 and 15 μ M) for 24 h. Scale bars, 100 μ m. GSDMD, gasdermin D; NLRP3, leucine-rich repeat-containing family pyrin domain-containing 3; NSA, necrosulfonamide.

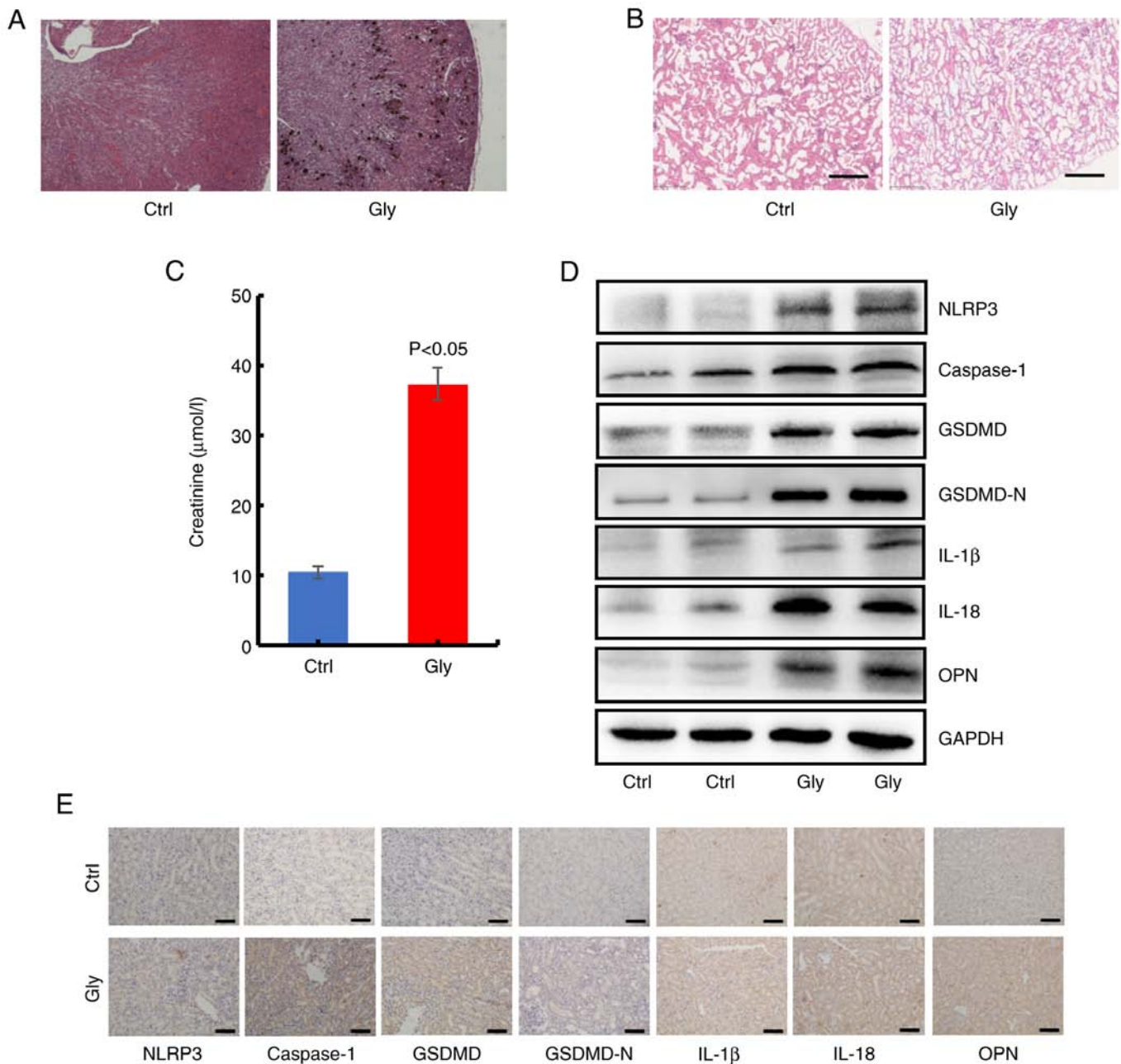


Figure 7. GSDMD mediates oxalate crystal-related pyroptosis *in vivo*. (A) Von Kossa staining revealed oxalate crystals in kidney of mice treated with Gly. (B) Haematoxylin and eosin staining demonstrated renal epithelial cell swelling, renal tubule edema and neutrophil infiltration in Gly treated mice. Scale bars, 50 μ m. (C) Serum creatinine level of Gly-treated mice was examined by creatinine assay (n=6). (D) Western blot analysis of indicated proteins in NLRP3-GSDMD pathway in oxalated crystal mice. (E) The expression of same proteins was detected through immunohistochemical assays in mice. Scale bars, 50 μ m. GSDMD, gasdermin D; Gly, glyoxylic acid; NLRP3, leucine-rich repeat-containing family pyrin domain-containing 3; OPN, osteopontin; Ctrl, control.

demonstrated that calcium oxalate crystals could result in injury in renal tubular epithelial cells (31,32). A previous study conducted by the authors demonstrated that oxalate could reduce the cell viability in rat renal tubular epithelial cells (14). It was proved that ROS-mediated NLRP3 inflammasome activation was involved in the onset and progression of calcium oxalate stones (21,33). In the present study, it was revealed that oxalate-induced activation of NLRP3 inflammasome and overexpression of caspase-1 could be inhibited by NAC. Consistent with previous studies, the present results confirmed that oxalate could induce the activation of NLRP3 pathway in HK-2 cells, which was mediated by ROS production. However,

the type and mechanism of oxalate-treated HK-2 cell injury had not been fully clarified.

A previous study demonstrated that inflammasome-dependent pyroptosis was a kind of programmed cell death (18). Both pyroptosis and apoptosis constitute programmed cell death mechanisms, but with the in-depth studies on the mechanism and ultrastructural feature of pyroptosis, the differences of pyroptosis and apoptosis were gradually realized (26). A small number of studies investigated the molecular mechanisms of NLRP3-mediated pyroptosis in calcium oxalate kidney stones (21,22); however, the specific morphological characteristic of pyroptosis in oxalate-induced crystals was

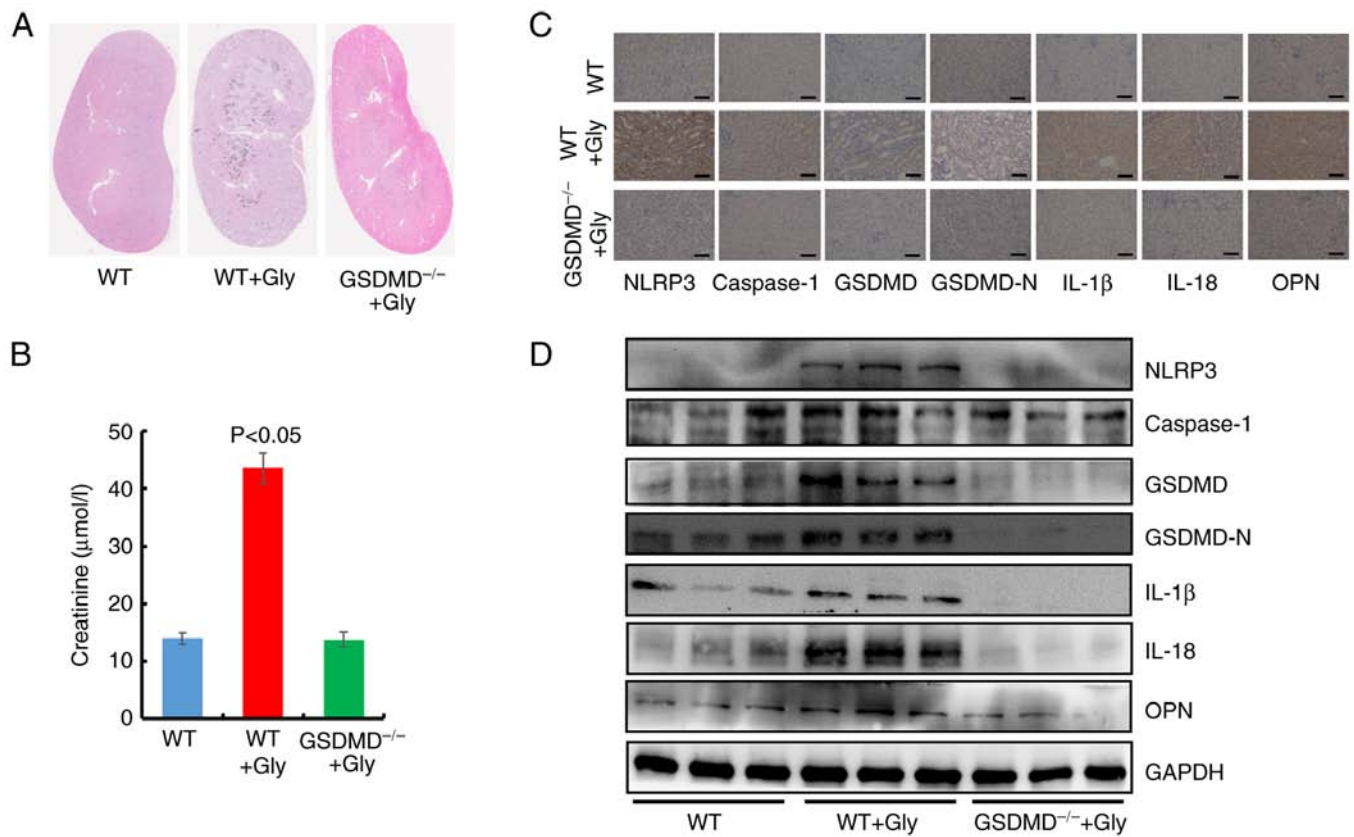


Figure 8. GSDMD deficiency alleviates formation of oxalate crystals in *GSDMD*^{-/-} mice. (A) Oxalate crystals formation was observed through Von Kossa staining in kidney of WT mice and *GSDMD*^{-/-} mice treated with Gly. (B) Serum creatinine levels were detected in WT mice and *GSDMD*^{-/-} mice treated with Gly (n=6). (C) Immunohistochemical examination of indicated proteins in NLRP3-GSDMD pathway in Gly-treated WT mice and *GSDMD*^{-/-} mice. Scale bars, 50 μm. (D) The contents of the same proteins were analyzed by western blot analysis. GSDMD, gasdermin D; WT, wild-type; Gly, glyoxylic acid; NLRP3, leucine-rich repeat-containing family pyrin domain-containing 3; OPN, osteopontin.

still not reported. Liu *et al* (34) identified a series of characteristic morphological changes of pyroptosis in human primary gingival epithelial cells, including swollen cells, large bubbles in the cytoplasm, membrane pores formation and structural changes in other organelles. Similarly, the results of the present study revealed that oxalate could induce autophagosome formation, mitochondrial damage and rough endoplasmic reticulum damage in HK-2 cells. In addition, several studies also demonstrated that ultrastructural changes of pyroptosis were induced by different factors in macrophages and cancer cells (18,35). Membrane pore was the most typical feature to distinguish pyroptosis from apoptosis (25). In the present study, the results exhibited the formation of membrane pores and cytosolic vacuoles in oxalate-induced injury in HK-2 cells, in accordance with a previous study in which calcium oxalate crystals-treated dendritic cells were investigated (7). Apart from the aforementioned ultrastructural changes, the present study also uncovered that oxalate crystals were devoured and microvilli in the free surface of oxalate-treated HK-2 cells. Analogous subcellular morphological changes were detected in calcium oxalate crystals-treated bone marrow-derived dendritic cells and tubular epithelial cells (7). In summary, the features of oxalate-induced HK-2 cell injury were attributed to NLRP3 inflammasome-mediated pyroptosis. The ultrastructural changes demonstrated in the present study partially explained HK-2 cell injury caused by oxalate from the perspective of micromorphology.

Pyroptosis mainly includes the caspase-1-mediated classical pyroptosis pathway and caspase-4/5/11-mediated non-classical pyroptosis pathway (25). In the classical pyroptosis pathway, various factors firstly activate recognition receptors (such as NLRP3 and NLRP1) on cell membrane, and subsequently, the corresponding inflammasome cleaves the procaspase-1 into its mature form caspase-1 (15). GSDMD, a member of gasdermin protein family, is the performer of cell pyroptosis. Caspase-1 could cleave GSDMD into its mature form GSDMD-N, which mediates the formation of membrane pores (18). Meanwhile, multiple GSDMD-N molecules are involved in the formation of a membrane pore (20). A previous study confirmed the role of GSDMD and GSDMD-N in cell pyroptosis (19). In the present study, it was also demonstrated that oxalate treatment could activate NLRP3-GSDMD signaling and increase the levels of GSDMD and GSDMD-N in HK-2 cells. Furthermore, inhibitor of GSDMD-N could ameliorate oxalate-induced cell pyroptosis *in vitro* and *in vivo*. Surprisingly, it was initially observed that GSDMD deletion dramatically suppressed oxalate crystals accumulation in the kidney of *GSDMD*^{-/-} mice treated with Gly, which suggested the significance of GSDMD in formation of oxalate crystals. Moreover, GSDMD itself was likely to possess a crucial function in oxalate crystal formation. Collectively, these findings illustrated that GSDMD was involved in the onset and progression of calcium oxalated kidney stone. Nevertheless, the direct role and intensive mechanism of GSDMD in

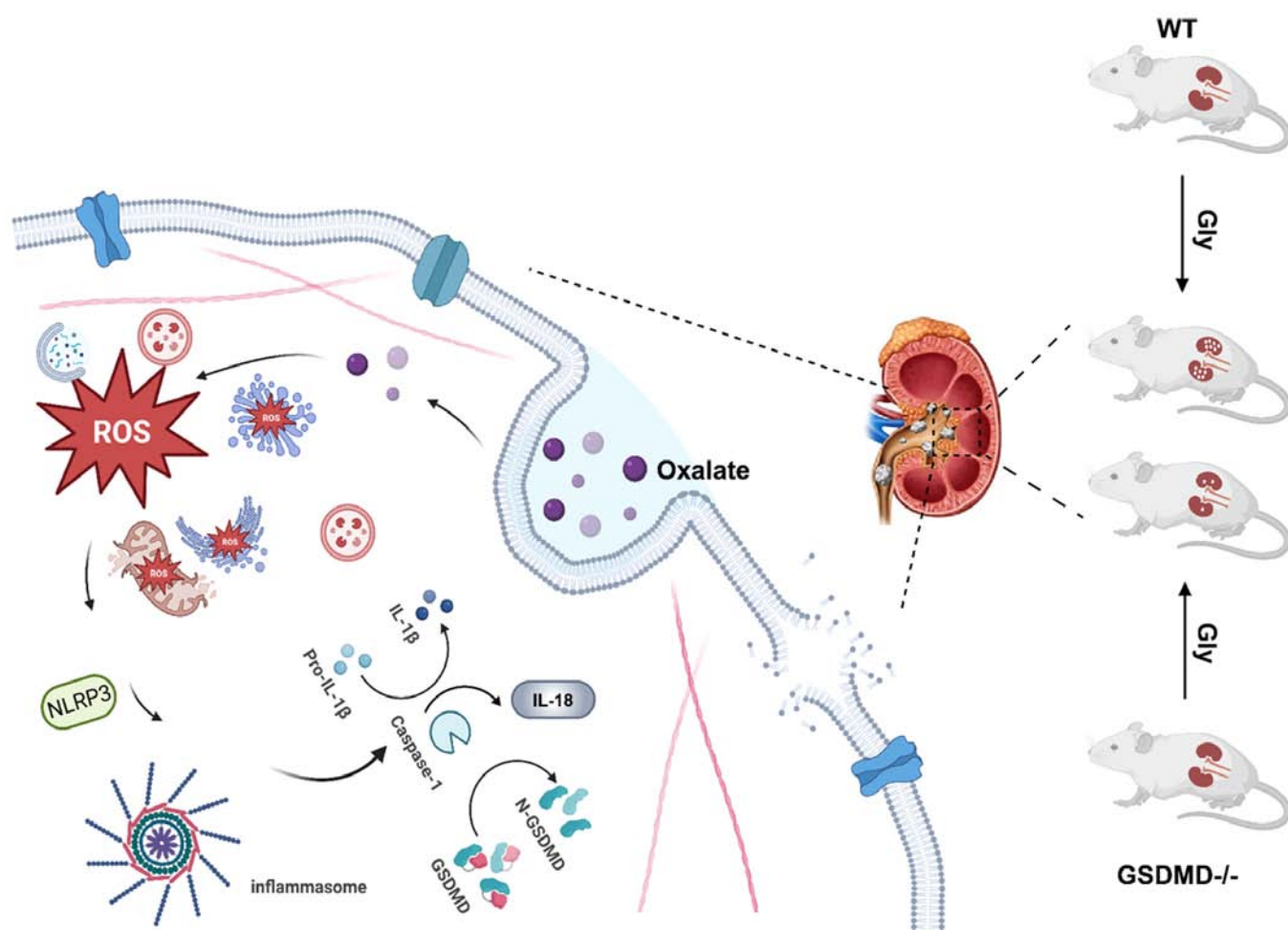


Figure 9. The schematic diagram describing the role of NLRP3-GSDMD signaling in oxalate-induced renal pyroptotic injury and crystal formation. NLRP3, leucine-rich repeat-containing family pyrin domain-containing 3; GSDMD, gasdermin; WT, wild-type; Gly, glyoxylic acid; ROS, reactive oxygen species.

oxalated-induced crystal formation and cell injury will be further investigated.

In conclusion, the present study confirmed that ROS-mediated NLRP3-GSDMD signaling pathway was involved in oxalate-induced injury in HK-2 cells. Importantly, the results deciphered the ultrastructural injury in oxalate-treated HK-2 cells, which was consistent with the typical cell pyroptosis. Moreover, GSDMD and its cleavage form GSDMD-N were associated with the oxalate-induced disruption of membrane integrity in HK-2 cells. Particularly, GSDMD knock down obviously inhibited formation of oxalate calcium crystals in mice, which suggested that plays an important role in the oxalate-induced renal injury and formation of oxalate calcium crystals (Fig. 9). The findings of the present study provided a new target for prevention and treatment of oxalate nephropathy and oxalate calcium stones. However, the intensive mechanisms of GSDMD-mediated renal injury in formation of oxalate calcium still need to be investigated. Moreover, determining how to repair this injury will contribute to inhibit the formation of oxalate calcium crystals.

Acknowledgements

Not applicable.

Funding

The present study was supported by the National Natural Science Foundation of China (grant no. 82070725), the Science and Technology Project of Tianjin (grant no. 17ZXMFSY00060), the Key Laboratory Fund Project of the Second Hospital of Tianjin Medical University (grant no. 2017ZDSYS14) and the Education Commission Research Project of Tianjin (grant no. 2017KJ208).

Availability of data and materials

The datasets used and/or analyzed during the current study are available from the corresponding author on reasonable request.

Authors' contributions

YC, LC and SQ designed the experiments. SY, HK, QW, SC and XW performed the experiments. YC, SY and HK conceived the project and analyzed the data. YC, LC and SQ wrote and revised the paper. SQ provided funding. YC and SQ confirm the authenticity of all the raw data. All authors contributed to the article, and read and approved the final version of the manuscript.

Ethics approval and consent to participate

The maintenance, treatment and experiments regarding the mice were approved by the Animal Ethics Committee at the Second Hospital of Tianjin Medical University (Tianjin, China).

Patient consent for publication

Not applicable.

Competing interests

The authors declare that they have no competing interests.

References

- Thongprayoon C, Krambeck AE and Rule AD: Determining the true burden of kidney stone disease. *Nat Rev Nephrol* 16: 736-746, 2020.
- Fontenelle LF and Sarti TD: Kidney stones: Treatment and prevention. *Am Fam Physician* 99: 490-496, 2019.
- Mitchell T, Kumar P, Reddy T, Wood KD, Knight J, Assimos DG and Holmes RP: Dietary oxalate and kidney stone formation. *Am J Physiol Renal Physiol* 316: F409-F413, 2019.
- Crivelli JJ, Mitchell T, Knight J, Wood KD, Assimos DG, Holmes RP and Fargue S: Contribution of dietary oxalate and oxalate precursors to urinary oxalate excretion. *Nutrients* 13: 62, 2020.
- Knoll T, Steidler A, Trojan L, Sagi S, Schaaf A, Yard B, Michel MS and Alken P: The influence of oxalate on renal epithelial and interstitial cells. *Urol Res* 32: 304-309, 2004.
- Song Q, Liao W, Chen X, He Z, Li D, Li B, Liu J, Liu L, Xiong Y, Song C and Yang S: Oxalate activates autophagy to induce ferroptosis of renal tubular epithelial cells and participates in the formation of kidney stones. *Oxid Med Cell Longev* 2021: 6630343, 2021.
- Mulay SR, Kulkarni OP, Rupanagudi KV, Migliorini A, Darisipudi MN, Vilaysane A, Muruve D, Shi Y, Munro F, Liapis H and Anders HJ: Calcium oxalate crystals induce renal inflammation by NLRP3-mediated IL-1 β secretion. *J Clin Invest* 123: 236-246, 2013.
- Joshi S, Wang W, Peck AB and Khan SR: Activation of the NLRP3 inflammasome in association with calcium oxalate crystal induced reactive oxygen species in kidneys. *J Urol* 193: 1684-1691, 2015.
- Kim YG, Kim SM, Kim KP, Lee SH and Moon JY: The role of inflammasome-dependent and inflammasome-independent NLRP3 in the kidney. *Cells* 8: 1389, 2019.
- Komada T and Muruve DA: The role of inflammasomes in kidney disease. *Nat Rev Nephrol* 15: 501-520, 2019.
- Darisipudi MN, Thomasova D, Mulay SR, Brech D, Noessner E, Liapis H and Anders HJ: Uromodulin triggers IL-1 β -dependent innate immunity via the NLRP3 inflammasome. *J Am Soc Nephrol* 23: 1783-1789, 2012.
- Liu P, Zhang Z and Li Y: Relevance of the pyroptosis-related inflammasome pathway in the pathogenesis of diabetic kidney disease. *Front Immunol* 12: 603416, 2021.
- Kelley N, Jeltema D, Duan Y and He Y: The NLRP3 inflammasome: An overview of mechanisms of activation and regulation. *Int J Mol Sci* 20: 3328, 2019.
- Qi S, Wang Q, Xie B, Chen Y, Zhang Z and Xu Y: P38 MAPK signaling pathway mediates COM crystal-induced crystal adhesion change in rat renal tubular epithelial cells. *Urolithiasis* 48: 9-18, 2020.
- Shi J, Gao W and Shao F: Pyroptosis: Gasdermin-mediated programmed necrotic cell death. *Trends Biochem Sci* 42: 245-254, 2017.
- Liu J, Yang K, Jin Y, Liu Y, Chen Y, Zhang X, Yu S, Song E, Chen S, Zhang J, *et al*: H3 relaxin protects against calcium oxalate crystal-induced renal inflammatory pyroptosis. *Cell Prolif* 53: e12902, 2020.
- Ding T, Zhao T, Li Y, Liu Z, Ding J, Ji B, Wang Y and Guo Z: Vitexin exerts protective effects against calcium oxalate crystal-induced kidney pyroptosis in vivo and in vitro. *Phytomedicine* 86: 153562, 2021.
- He WT, Wan H, Hu L, Chen P, Wang X, Huang Z, Yang ZH, Zhong CQ and Han J: Gasdermin D is an executor of pyroptosis and required for interleukin-1 β secretion. *Cell Res* 25: 1285-1298, 2015.
- Liu X, Zhang Z, Ruan J, Pan Y, Magupalli VG, Wu H and Lieberman J: Inflammasome-activated gasdermin D causes pyroptosis by forming membrane pores. *Nature* 535: 153-158, 2016.
- Sborgi L, Rühl S, Mulvihill E, Pipercevic J, Heilig R, Stahlberg H, Farady CJ, Müller DJ, Broz P and Hiller S: GSDMD membrane pore formation constitutes the mechanism of pyroptotic cell death. *EMBO J* 35: 1766-1778, 2016.
- Song Z, Zhang Y, Gong B, Xu H, Hao Z and Liang C: Long noncoding RNA LINC00339 promotes renal tubular epithelial pyroptosis by regulating the miR-22-3p/NLRP3 axis in calcium oxalate-induced kidney stone. *J Cell Biochem* 120: 10452-10462, 2019.
- Gan XG, Wang ZH and Xu HT: Mechanism of miRNA-141-3p in calcium oxalate-induced renal tubular epithelial cell injury via NLRP3-mediated pyroptosis. *Kidney Blood Press Res* 47: 300-308, 2022.
- Livak KJ and Schmittgen TD: Analysis of relative gene expression data using real-time quantitative PCR and the 2(-Delta Delta C(T)) method. *Methods* 25: 402-408, 2001.
- Zhou R, Yazdi AS, Menu P and Tschopp J: A role for mitochondria in NLRP3 inflammasome activation. *Nature* 469: 221-225, 2011.
- Vande Walle L and Lamkanfi M: Pyroptosis. *Curr Biol* 26: R568-R572, 2016.
- D'Arcy MS: Cell death: A review of the major forms of apoptosis, necrosis and autophagy. *Cell Biol Int* 43: 582-592, 2019.
- Wang S, Du P, Zhang N, Liu J, Tang X, Zhao Q and Yang Y: Oligomeric proanthocyanidins protect against HK-2 cell injury induced by oxalate and calcium oxalate monohydrate crystals. *Urolithiasis* 44: 203-210, 2016.
- Moe OW: Kidney stones: Pathophysiology and medical management. *Lancet* 367: 333-344, 2006.
- Khan SR, Canales BK and Dominguez-Gutierrez PR: Randall's plaque and calcium oxalate stone formation: Role for immunity and inflammation. *Nat Rev Nephrol* 17: 417-433, 2021.
- Lv P, Liu H, Ye T, Yang X, Duan C, Yao X, Li B, Tang K, Chen Z, Liu J, *et al*: XIST inhibition attenuates calcium oxalate nephrocalcinosis-induced renal inflammation and oxidative injury via the miR-223/NLRP3 pathway. *Oxid Med Cell Longev* 2021: 1676152, 2021.
- Fong-Ngern K, Vinaiphath A and Thongboonkerd V: Microvillar injury in renal tubular epithelial cells induced by calcium oxalate crystal and the protective role of epigallocatechin-3-gallate. *FASEB J* 31: 120-131, 2017.
- Liu H, Ye T, Yang X, Liu J, Jiang K, Lu H, Xia D, Peng E, Chen Z, Sun F, *et al*: H19 promote calcium oxalate nephrocalcinosis-induced renal tubular epithelial cell injury via a ceRNA pathway. *EBioMedicine* 50: 366-378, 2019.
- Yu L, Gan X, Liu X and An R: Calcium oxalate crystals induces tight junction disruption in distal renal tubular epithelial cells by activating ROS/Akt/p38 MAPK signaling pathway. *Ren Fail* 39: 440-451, 2017.
- Liu J, Wang Y, Meng H, Yu J, Lu H, Li W, Lu R, Zhao Y, Li Q and Su L: Butyrate rather than LPS subverts gingival epithelial homeostasis by downregulation of intercellular junctions and triggering pyroptosis. *J Clin Periodontol* 46: 894-907, 2019.
- Yu J, Li S, Qi J, Chen Z, Wu Y, Guo J, Wang K, Sun X and Zheng J: Cleavage of GSDME by caspase-3 determines lobaplatin-induced pyroptosis in colon cancer cells. *Cell Death Dis* 10: 193, 2019.



Copyright © 2023 Chen *et al.* This work is licensed under a Creative Commons Attribution-NonCommercial-NoDerivatives 4.0 International (CC BY-NC-ND 4.0) License.